Development 140, 3977-3985 (2013) doi:10.1242/dev.097071

Hemogenic endothelium specification and hematopoietic stem cell maintenance employ distinct Scl isoforms

Fenghua Zhen[1,*], Yahui Lan[1,*], Bo Yan[1], Wenqing Zhang[2,‡] and Zilong Wen[1,‡]

SUMMARY

Recent studies have shown that nascent hematopoietic stem cells (HSCs) derive directly from the ventral aortic endothelium (VAE) via endothelial to hematopoietic transition (EHT). However, whether EHT initiates from a random or predetermined subpopulation of VAE, as well as the molecular mechanism underlying this process, remain unclear. We previously reported that different zebrafish *stem cell leukemia* (*scl*) isoforms are differentially required for HSC formation in the ventral wall of the dorsal aorta. However, the exact stage at which these isoforms impact HSC development was not defined. Here, using *in vivo* time-lapse imaging of *scl* isoform-specific reporter transgenic zebrafish lines, we show that prior to EHT *scl-β* is selectively expressed in hemogenic endothelial cells, a unique subset of VAE cells possessing hemogenic potential, whereas *scl-α* is expressed later in nascent HSCs as they egress from VAE cells. In accordance with their expression, loss-of-function studies coupled with *in vivo* imaging analysis reveal that *scl-β* acts earlier to specify hemogenic endothelium, which is later transformed by *runx1* into HSCs. Our results also reveal a previously unexpected role of *scl-α* in maintaining newly born HSCs in the aorta-gonads-mesonephros. Thus, our data suggest that a defined hemogenic endothelial population preset by *scl-β* supports the deterministic emergence of HSCs, and unravel the cellular mechanisms by which *scl* isoforms regulate HSC development.

KEY WORDS: Zebrafish, Scl, Tal1, Hemogenic endothelium, Hematopoietic stem cells

INTRODUCTION

The formation of multipotent hematopoietic stem cells (HSCs) during development is crucial for the establishment of the blood system (Orkin and Zon, 2008). Understanding the developmental pathway through which HSCs arise and the associated molecular mechanisms would therefore provide new insights into stem cell biology and HSC-based regenerative therapies. Recent studies on cultured mouse mesoderm cells or isolated hemangioblasts have shown that the first pool of HSCs is directly initiated from endothelial cells through a specialized intermediate, termed the hemogenic endothelium, without apparent cell division (Eilken et al., 2009; Lancrin et al., 2009). These observations are supported by *in vivo* time-lapse confocal imaging that has captured the emergence of HSCs from the ventral aortic endothelial (VAE) cells through an endothelial to hematopoietic transition (EHT) in mouse aorta explants and in intact zebrafish embryos (Bertrand et al., 2010; Boisset et al., 2010; Kissa and Herbomel, 2010; Lam et al., 2010). Yet, whether EHT initiates stochastically from the uniform endothelial cells or deterministically from a specialized hemogenic endothelial population is not known. After EHT, the nascent HSCs either form intra-arterial clusters (mouse) or remain in the subaortic mesenchymal region (zebrafish) before they are released into the circulation to colonize downstream hematopoietic organs (Kissa et al., 2008; Bertrand et al., 2010; Kissa and Herbomel, 2010; Lam et al., 2010). The molecular control over the post-EHT development of HSCs in the aorta-gonads-mesonephros (AGM) remains largely unexplored, with only one study showing the extrinsic regulation of AGM HSC proliferation by Il-3 (Robin et al., 2006).

The basic helix-loop-helix transcription factor stem cell leukemia (SCL, also known as TAL1) is a crucial regulator of both primitive and definitive hematopoiesis in teleosts and mammals (Robb et al., 1995; Shivdasani et al., 1995; Porcher et al., 1996; Robb et al., 1996; Dooley et al., 2005; Patterson et al., 2005). The expression of SCL is highly enriched in hematopoietic and endothelial cells, as well as in the central nervous system (Green et al., 1991; Green et al., 1992; Hwang et al., 1993; Kallianpur et al., 1994; Gering et al., 1998; Zhang and Rodaway, 2007). Loss-of-function of SCL impairs yolk sac hematopoiesis (Robb et al., 1995; Shivdasani et al., 1995), HSC formation and subsequent hematopoietic lineage differentiation (Porcher et al., 1996; Robb et al., 1996), as well as the vascular remodeling of the yolk sac endothelium (Visvader et al., 1998). In zebrafish, *scl* has been shown to play a similar role in regulating primitive hematopoiesis, HSC development and dorsal aorta formation (Dooley et al., 2005; Patterson et al., 2005). Recent studies have identified multiple *scl* isoforms: the full-length *scl-α* isoform and the N-terminal-truncated *scl-β* isoform. It was found that *scl-β* is essential whereas *scl-α* is dispensable for HSC generation in the ventral wall of the dorsal aorta (VDA) (Qian et al., 2007; Ren et al., 2010), which is the zebrafish equivalent of the AGM (the term AGM will be used hereafter) (Burns et al., 2005; Gering and Patient, 2005; Murayama et al., 2006; Jin et al., 2007). Despite the demonstration of a differential requirement for *scl* isoforms in definitive hematopoiesis, the developmental step at which *scl-β* acts to influence HSC formation remains to be elucidated. Whether *scl-α* has any essential role beyond the stage of AGM HSC generation is also unclear.

In this study, we generated *scl-α* and *-β* isoform-specific reporter transgenic zebrafish lines in which the dynamic expression of these two isoforms could be followed individually *in vivo*. Through time-

[1]State Key Laboratory of Molecular Neuroscience, Center of Systems Biology and Human Health, Division of Life Science, Hong Kong University of Science and Technology, Clear Water Bay, Kowloon, Hong Kong, P.R. China. [2]Key Laboratory of Zebrafish Modeling and Drug Screening for Human Diseases of Guangdong Higher Education Institutes, Department of Cell Biology, Southern Medical University, Guangzhou 510515, P.R. China.

*These authors contributed equally to this work
‡Authors for correspondence (zzwwqq@smu.edu.cn; zilong@ust.hk)

Accepted 17 July 2013

lapse imaging with these transgenics, we showed that prior to EHT, *scl-β* is predominantly expressed in a subset of VAE cells. These *scl-β*$^{+}$, but not *scl-β*$^{–}$, VAE cells were traced to transform into HSCs in the AGM, suggesting that *scl-β* expression marks hemogenic endothelial cells. By contrast, the expression of *scl-α* was not detectable in VAE cells but initiated later, in budding HSCs, and gradually accumulated in these cells thereafter. Loss-of-function studies combined with high-resolution *in vivo* time-lapse imaging analysis showed that knocking down *scl* isoforms elicited a phenotype that was consistent with their expression patterns. Unlike *runx1* knockdown embryos with abortive EHT, *scl-β* knockdown embryos selectively lost hemogenic endothelial cells, thus defining a role for *scl-β* in hemogenic endothelium specification. *scl-α*, however, is required later for HSC maintenance in the AGM, as demonstrated by intact hemogenic endothelium specification and EHT but post-EHT loss of AGM HSCs in *scl-α* knockdown embryos.

Taken together, our results suggest a defined hemogenic endothelial subpopulation preset by *scl-β* in the aortic endothelium that governs the deterministic emergence of EHT, and unravel the cellular mechanisms by which *scl* isoforms regulate AGM HSC development.

MATERIALS AND METHODS

Zebrafish husbandry

Zebrafish were mated and embryos were raised and staged according to standard protocols (Kimmel et al., 1995). Zebrafish strains AB, *Tg*(*scl-β:d2eGFP; scl-α:DsRed*), *Tg*(*scl-β:d2eGFP*), *Tg*(*scl-α:DsRed*), *Tg*(*kdrl:eGFP*) (Jin et al., 2005), *Tg*(*kdrl:Ras-mCherry*)^{s896} (Lee et al., 2009), *Tg*(*cmyb:eGFP*) (North et al., 2007), *Tg*(*CD41:eGFP*) (Lin et al., 2005) and *runx1*^{w84x} (Jin et al., 2009; Sood et al., 2010) were used in this study.

Generation of PAC targeting constructs

The *scl* PAC clone (BUSM-129I22) was purchased from the Chris T. Amemiya laboratory via ZFIN (www.zfin.org) and transformed by electroporation into *E. coli* strain DH10B. The transformants were selected by kanamycin resistance and introduced into electroporation-competent cells. To construct the *scl* PAC used to generate *Tg*(*scl-β:d2eGFP; scl-α:DsRed*) (Fig. 1B), we first generated the DsRed expression cassette. The DsRed coding sequences and SV40 poly(A) signal (Clontech, pDsRed-Express-1) and a chloramphenicol selection cassette (CSC) flanked by two FRT sites (Gene Bridges, FRT-bg2-cm-FRT) were PCR amplified and sequentially ligated into the pGEM-Teasy vector. To generate the exon 1 recombination construct, two DNA fragments of identical sequence to (AL592495) 37932-39209 and 39209-40520 were amplified by PCR, and an enzyme bridge (*Eco*RI-*Eco*RV-*Hin*dIII-*Sal*I-*Xho*I) between these two fragments was

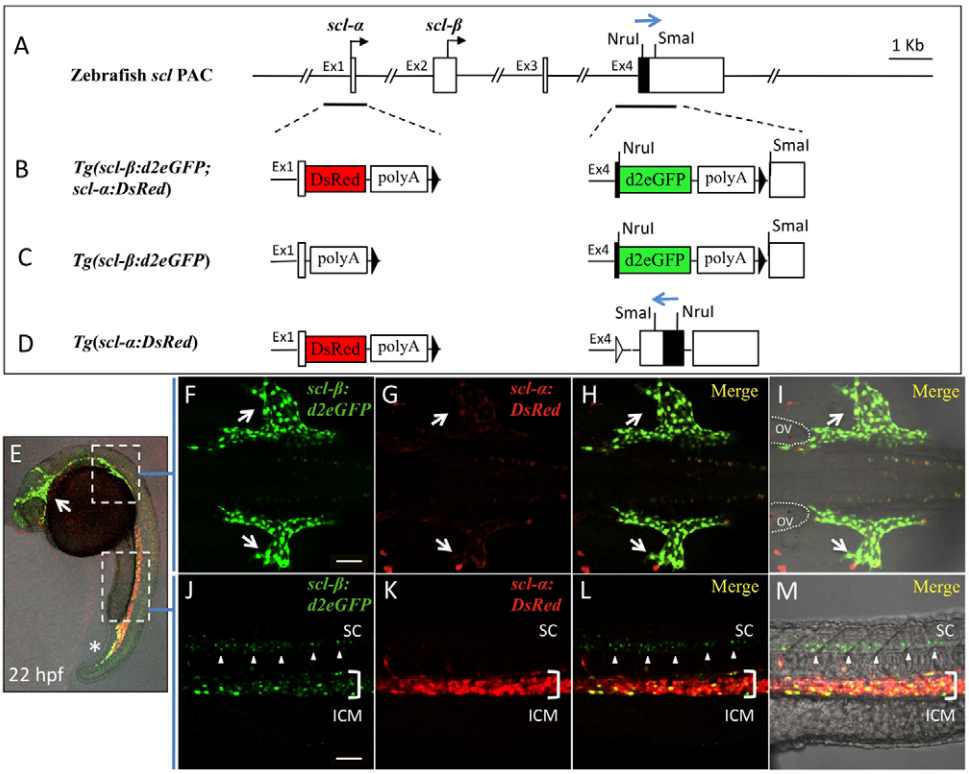

Fig. 1. Generation of *scl* transgenic lines and expression of *d2eGFP* and *DsRed* coincides with that of the endogenous *scl-β* and *scl-α* isoforms. (**A**) The structure of the zebrafish *scl* locus in the PAC clone BUSM-129I22. The transcription start sites of *scl-α* and *scl-β* are indicated (black arrows). The black box in exon 4 represents sequences encoding the basic helix-loop-helix (bHLH) domain. (**B-D**) The modified *scl* PAC used to generate *Tg*(*scl-β:d2eGFP; scl-α:DsRed*), *Tg*(*scl-β:d2eGFP*) and *Tg*(*scl-α:DsRed*). DsRed, an SV40 polyadenylation signal and a remaining FRT site were inserted behind exon 1 (B,D). d2eGFP, an SV40 polyadenylation signal and a remaining FRT site were inserted in exon 4 (B,C). The transcription activity of *scl-α* was interrupted by an SV40 polyadenylation signal immediately after exon 1 (C), whereas Scl-β expression was disrupted by the reversal of the protein coding sequences in exon 4 (D, blue arrow). (**E-M**) Expression of fluorescent reporter proteins in a 22 hpf *Tg*(*scl-β:d2eGFP; scl-α:DsRed*) embryo. *Scl-β:d2eGFP* is largely expressed in the head vasculature (E, arrow), the developing common cardinal vein (CCV) (F-I, arrows) and posterior part of the posterior blood island (PBI) (E, asterisk). By contrast, *scl-α:DsRed* is restricted in the intermediate cell mass (ICM) (J-M, bracket). (F-I) Higher magnification of d2eGFP and DsRed expression in the anterior lateral plate mesoderm region. D2eGFP is highly expressed in endothelial cells of the CCV across the yolk sac (arrows), whereas DsRed is almost undetected. (J-M) Higher magnification of d2eGFP and DsRed expression in the ICM region. DsRed is largely expressed in erythrocytes of the ICM, whereas d2eGFP is less expressed in ICM but dominant in neurons of the whole trunk segment of the spinal cord (arrowheads). The embryos are shown in lateral (E,J-M) or dorsal (F-I) views, with anterior to the left. ov, otic vesicle; sc, spinal cord. Scale bars: 50 μm.

introduced by stepwise PCR amplification. The fragment 37932-*Eco*RI-*Eco*RV-*Hin*dIII-*Sal*I-*Xho*I-40520 was then cloned into the pBluescript SK vector. We then inserted the DsRed expression cassette (DsRed-SV40-FRT-CSC-FRT) into the *Eco*RI/*Xho*I sites of the exon 1 recombination construct. The DNA fragment 37932-DsRed expression cassette-40520 was then digested and used for homologous recombination. Similarly, the fragment d2eGFP (Clontech, pd2eGFP)-SV40-FRT-CSC-FRT was generated and inserted into the *Nru*I/*Sma*I sites of the exon 4 recombination construct (pBluescript SK-45292-49127). The DNA fragment 45292-d2eGFP expression cassette-49127 was then digested and used for homologous recombination. To construct the *scl* PAC used to generate *Tg*(*scl-β:d2eGFP*) (Fig. 1C), the fragment SV40-FRT-CSC-FRT was inserted into the exon 1 recombination construct. To construct the *scl* PAC used to generate *Tg*(*scl-α:DsRed*) (Fig. 1D), the DNA sequences 45346-46973, LoxP-CSC-LoxP, reversed DNA sequences of 46931-47476 and 47472-49003 were sequentially ligated into pBluescript SK to generate the exon 4 recombination construct. Finally, the DNA fragment 45346-CSC-(47476-46391)-49003 was digested and used for homologous recombination.

Homologous recombination and PAC injection

To introduce targeting recombination constructs into the designated site in the PAC, we performed a recombinase-mediated recombination modified from previous studies (Yang et al., 2006). The linearized targeting recombination constructs described above were transformed into *E. coli* DH10B cells containing both the original *scl* PAC and pGETrec (recombinase) plasmid by electroporation. The recombination was induced by adding L-arabinose during 1 hour of culture, then recombinants were selected by growth under both kanamycin and chloramphenicol selection conditions. After confirmation that the positive recombinants harbored the correct targeting constructs, the CSC fragment was removed by Flp-mediated excision. Prior to microinjection, the modified PAC was digested by I-*Sce*I for 1 hour (Rembold et al., 2006). A final concentration of 50 ng/μl linearized PAC was injected into one-cell stage embryos, which were raised to adulthood to generate transgenics.

Morpholinos (MOs) and injection

scl MOs (Gene Tools) were used as previously described (Qian et al., 2007); 3 ng *scl-α* MO (5′-GCTCGGATTTCAGTTTTTCCATCAT-3′) and 8 ng *scl-β* MO (5′-GCGGACTCAACTGCACCATTCGAGT-3′) were injected (Burns et al., 2005). A mixture containing a final concentration of 0.6 mM *runx1* MO3 (5′-TGTTAAACTCACGTCGTGGCTCTC-3′) and 1 mM *runx1* MO5 (5′-AATGTGTAAACTCACAGTGTAAAGC-3′) was prepared prior to microinjection (Burns et al., 2005). MOs were injected into one-cell stage embryos and the injected embryos were raised to the required developmental stages.

Whole-mount *in situ* hybridization (WISH) and antibody staining

Single (Qian et al., 2007) and double (Jin et al., 2007) WISH were performed as previously described. The protocol for single immunohistochemical staining (Qian et al., 2007) was also used to detect d2eGFP and Scl-β simultaneously. Goat anti-GFP (Abcam, Ab6658; 1:400) and rabbit Ab-Scl-C [made by ourselves (Qian et al., 2007); 1:50] were used as primary antibodies; anti-goat Alexa Fluor 488 (Invitrogen, A11055; 1:400) and anti-rabbit Alexa Fluor 555 (Invitrogen, A31572; 1:400) were used as secondary antibodies.

Time-lapse confocal microscopy

For time-lapse confocal microscopy, embryos were first anaesthetized in 0.02% tricaine in embryo water, then mounted in 0.5% low-melting agarose on a 35-mm plastic Petri dish (Iwaki), and covered with embryo water containing 0.02% tricaine. Embryos were examined using a Zeiss LSM 510 confocal microscope or an Olympus FluoView 1000 confocal microscope equipped with an environmental chamber to maintain temperature (28°C) and humidity. Confocal *z*-stacks of 3 μm steps were taken every 8-10 minutes, and 25-30 stacks were typically imaged for each embryo.

Processing of time-lapse confocal images

Raw data of time-lapse confocal imaging were analyzed using either LSM Image Browser (Zeiss) or FV10-ASW 2.0 Viewer (Olympus) software. Confocal planes at each time point were individually analyzed to select the most representative images and to perform the projection. The images after projection were exported and saved through time, then imported to generate a sequence file in SPOT Advanced software (SPOT Imaging Solutions). After annotation, the sequence file was exported as a .mov movie in QuickTime (Apple) format.

RESULTS

Generation of *scl-α* and *scl-β* isoform-specific reporter transgenic zebrafish lines

To visualize the dynamic expression of individual *scl* isoforms and provide clues as to the possible roles of these isoforms in the development of AGM HSCs, we created three stable *scl* transgenic zebrafish lines: a dual *scl* isoform reporter line *Tg*(*scl-β:d2eGFP; scl-α:DsRed*) (Fig. 1B), an *scl-β* reporter line *Tg*(*scl-β:d2eGFP*) (Fig. 1C), and an *scl-α* reporter line *Tg*(*scl-α:DsRed*) (Fig. 1D). To generate these lines, a P1 artificial chromosome (PAC) clone containing the zebrafish *scl* genomic locus was modified to express GFP and/or DsRed corresponding to the expression of *scl-β* and/or *scl-α* (Fig. 1A-D). A destabilized eGFP form (d2eGFP) with a shorter half-life of only 2 hours was used to minimize the carryover of fluorescent protein from the GFP-expressing ancestor cells to their non-GFP-expressing progeny, while a fast-folding version of DsRed (DsRed-Express) was implemented to minimize the signal retardation during dual-color imaging studies (Bevis and Glick, 2002).

We then examined the expression patterns of d2eGFP and DsRed in *Tg*(*scl-β:d2eGFP; scl-α:DsRed*) embryos (Fig. 1E-M), focusing on 22 hours postfertilization (hpf), when the spatial expression patterns of the endogenous isoforms clearly differ (Qian et al., 2007). At 22 hpf, *scl-β:d2eGFP* was predominantly expressed in the head vasculature (Fig. 1E, arrow), in endothelial cells of the developing common cardinal vein [a characteristic *scl-β*-expressing population that shows no expression of *scl-α* (Qian et al., 2007)] (Fig. 1E-I), and in the caudal part of the posterior blood island (Fig. 1E, asterisk). By contrast, the expression of *scl-α:DsRed* was restricted in the intermediate cell mass region (Fig. 1E,J-M). These results show that the expression of both transgenes coincides with that of the endogenous *scl-β* and *scl-α* isoforms as previously reported (Qian et al., 2007).

In addition, 5′-rapid amplification of cDNA ends (RACE) experiments confirmed that the *d2eGFP* and *DsRed* transcripts were initiated from the designated transcription start sites of the *scl-β* and *scl-α* isoforms, respectively (supplementary material Fig. S1A) (Qian et al., 2007). Consequently, a fusion protein between d2eGFP and the N-terminal 75 amino acids of Scl-β was produced, leading to the nuclear location of d2eGFP (supplementary material Fig. S1B). Moreover, double-staining experiments confirmed that d2eGFP and *DsRed* colocalize with the endogenous expression of Scl-β and *scl-α*, respectively (supplementary material Fig. S1C).

Taken together, these data indicate that the fluorescent reporter expression in the isoform-specific transgenic zebrafish lines faithfully mimics the endogenous expression of *scl-α* and *scl-β*.

scl-β$^+$ endothelial cells give rise to *scl-β*$^+$/*scl-α*$^+$ HSCs in the AGM

We then characterized the dynamic expression of the isoform-specific reporters by high-resolution *in vivo* time-lapse imaging during definitive hematopoiesis, specifically around the time that HSCs are born in the AGM region. Recent studies have delineated the emergence of HSC from the aortic floor by means of EHT, in which VAE cells bend and round up to become HSCs (Bertrand et

al., 2010; Kissa and Herbomel, 2010; Lam et al., 2010). Prior to EHT, which normally occurs between 32 and 60 hpf (Kissa and Herbomel, 2010), *scl-β:d2eGFP*, but not *scl-α:DsRed*, expression was clearly detected in a thin layer of cells lining the prospective AGM at ~25-26 hpf (Fig. 2A-C). These *scl-β:d2eGFP*$^+$/*scl-α:DsRed*$^-$ cells co-expressed an endothelial-specific transgene, *kdrl:Ras-mcherry* (Lee et al., 2009), indicating their endothelial identity (Fig. 2D-F). When the embryos developed to the stage of EHT, *scl-α:DsRed* began to be weakly expressed in the AGM and this expression was strictly restricted to *scl-β:d2eGFP*$^+$ cells, defining the transition of *scl-β:d2eGFP*$^+$ cells to *scl-β:d2eGFP*$^+$/*scl-α:DsRed*$^+$ cells. Along with the subsequent intensification of DsRed signals, these *scl-β:d2eGFP*$^+$/*scl-α:DsRed*$^+$ cells were seen to bend ventrally to become round cells, just as budding HSCs normally do (supplementary material Fig. S2). Consequently, by 36 hpf, the round *scl-β:d2eGFP*$^+$/*scl-α:DsRed*$^+$ cells were readily observable in the AGM (Fig. 2G-I). These cells displayed behavior characteristic of HSCs (Bertrand et al., 2010; Kissa and Herbomel, 2010; Lam et al., 2010): they normally remained in the subaortic space for 4-5 hours, during which time some underwent cell division, and subsequently entered the blood circulation through the axial vein (supplementary material Movie 1). Finally, these cells were observed to populate downstream hematopoietic tissues: the caudal hematopoietic tissue (CHT) (Murayama et al., 2006; Jin et al., 2007), thymus and kidney (supplementary material Fig. S3). To confirm the identity of these *scl-β:d2eGFP*$^+$/*scl-α:DsRed*$^+$ cells, we examined the expression of HSC-specific markers. They co-expressed two HSC-specific transgenes, *cmyb:eGFP* and *CD41:eGFP*, in the AGM (Fig. 2J-O), confirming that they are indeed HSCs.

Collectively, these data suggest that the differential expression of *scl* isoforms identifies two sequential cell populations in the AGM, with the earlier *scl-β:d2eGFP*$^+$ cells being hemogenic endothelium and later transiting to *scl-β:d2eGFP*$^+$/*scl-α:DsRed*$^+$ HSCs.

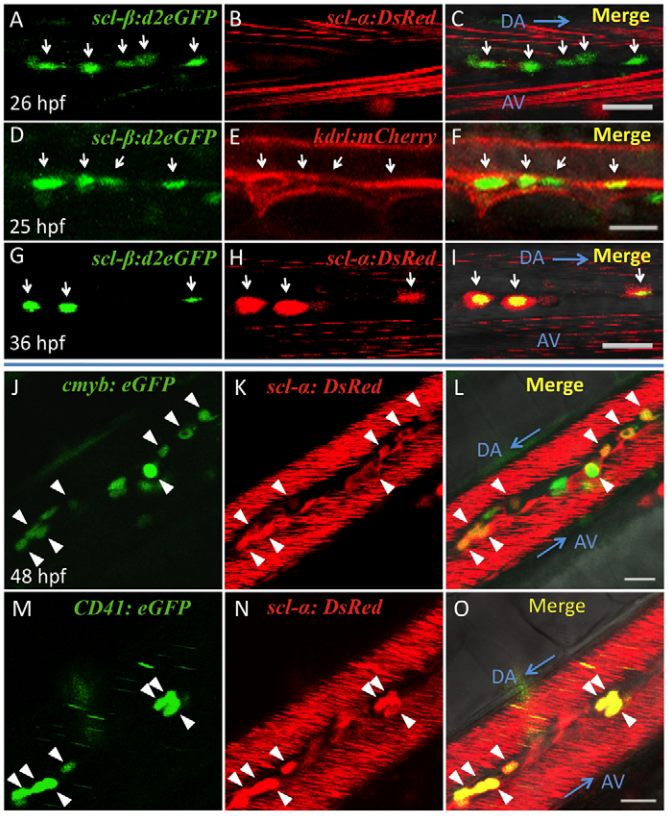

Fig. 2. Expression of *scl-β* and of *scl-α* in the AGM represent two sequential cell populations. (**A-C**) Expression of fluorescent proteins in the AGM of a 26 hpf *Tg*(*scl-β:d2eGFP; scl-α:DsRed*) zebrafish embryo. The *scl-β:d2eGFP* signals were detected lining the ventral side of the dorsal aorta, whereas expression of *scl-α:DsRed* was absent. (**D-F**) Expression of fluorescent proteins in the AGM of a 25 hpf *Tg*(*scl-β:d2eGFP; kdrl:Ras-mCherry*) embryo. *scl-β:d2eGFP* was co-expressed with *kdrl:Ras-mCherry* in endothelial cells. (**G-I**) Expression of fluorescent proteins in the AGM of a 36 hpf *Tg*(*scl-β:d2eGFP; scl-α:DsRed*) embryo. The *scl-β:d2eGFP* and *scl-α:DsRed* signals overlapped in the forming HSCs. Arrows in A-I indicate the cells in the AGM that express the corresponding fluorescent proteins. (**J-O**) *cmyb* or *CD41* (*itga2b*) is co-expressed with *scl-a* in AGM HSCs (arrowheads) of 48 hpf live *Tg*(*cmyb:eGFP; scl-α:DsRed*) embryos or 56 hpf live *Tg*(*CD41:eGFP; scl-α:DsRed*) embryos. Blue arrows indicate the direction of circulation. The red stripes in vessels are due to the rapid confocal scanning of circulating *scl-α:DsRed*$^+$ red blood cells. DA, dorsal aorta; AV, axial vein. Scale bars: 20 μm.

Expression of *scl-β* marks hemogenic endothelium

To further explore the relationship between the expression of *scl-β* and the hemogenic potential of VAE cells (which is defined here by the ability of these cells to become HSCs via EHT), we crossed the *Tg*(*scl-β:d2eGFP*) line with the *Tg*(*kdrl:Ras-mcherry*) line, which has been used to score all possible EHT events during HSC formation in the AGM (Lam et al., 2010). Time-lapse confocal imaging on *Tg*(*scl-β:d2eGFP; kdrl:Ras-mcherry*) embryos revealed that about half of *kdrl:Ras-mcherry*$^+$ VAE cells were also *scl-β:d2eGFP*$^+$ prior to EHT (25-28 hpf). These *scl-β:d2eGFP*$^+$/*kdrl:Ras-mcherry*$^+$ cells were of the typical elongated endothelial cell shape and were morphologically indistinguishable from the remaining *kdrl:Ras-mcherry*$^+$/*scl-β:d2eGFP*$^-$ population. During the observation period (from 28 to 54 hpf), the vast majority (~80%) of these *scl-β:d2eGFP*$^+$/*kdrl:Ras-mcherry*$^+$ cells underwent EHT to form HSCs (Fig. 3B-K; supplementary material Table S1, Movie 2). More importantly, of 46 EHT events observed in six embryos (supplementary material Table S1), all instances of EHT were initiated from *scl-β:d2eGFP*$^+$ endothelial cells, and none of the *scl-β:d2eGFP*$^-$ endothelial cells were observed to undergo EHT. These results suggest that early *scl-β* expression in the AGM uniquely and exclusively marks the hemogenic endothelium capable of producing HSCs via EHT.

scl-β is required for the specification of hemogenic endothelium

In light of our previous studies showing the requirement of *scl-β* for AGM HSC formation (Qian et al., 2007) and the above results illustrating the specific expression of *scl-β* in hemogenic VAE cells, we speculate that *scl-β* might regulate HSC formation by specifying hemogenic endothelium. To examine this possibility, we employed *in vivo* time-lapse imaging to track the transformation of endothelial cells into HSCs in embryos in which *scl-β* expression was inhibited by an *scl-β*-specific morpholino (MO) (Qian et al., 2007). Because the *scl-β* MO interfered with the translation of d2eGFP through recognizing the *scl* 5′UTR sequence in the *d2eGFP* transcript (supplementary material Fig. S1A), we could not evaluate the effect of MO knockdown in *Tg*(*scl-β:d2eGFP*) embryos; instead, *Tg*(*scl-α:DsRed; kdrl:eGFP*) embryos were used.

In *scl-β*-deficient embryos, we observed the fragmentation of a subset of *kdrl:eGFP*$^+$ VAE cells taking place before the onset of EHT (32 hpf) (Fig. 4B-D″; supplementary material Movie 3).

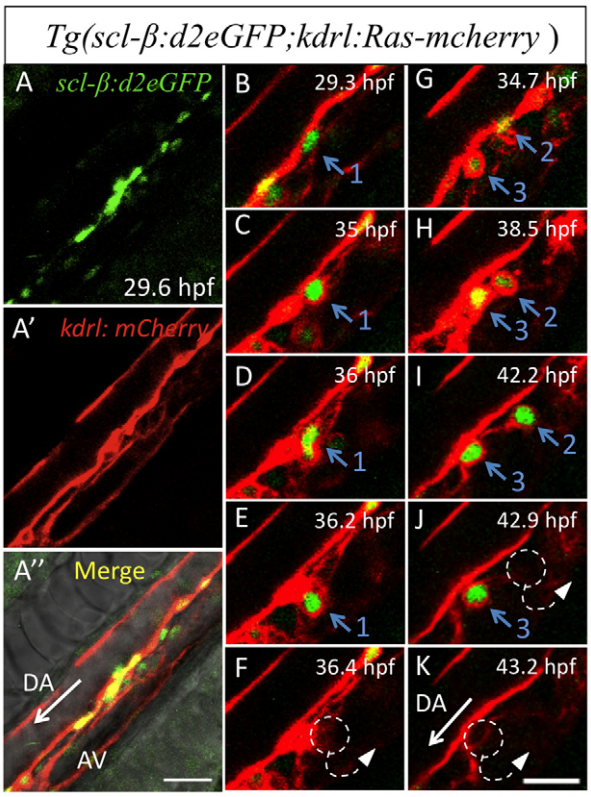

Fig. 3. Expression of *scl-β* labels hemogenic endothelium that undergoes EHT. Time-lapse confocal imaging of a live *Tg(scl-β:d2eGFP; kdrl:Ras-mcherry)* zebrafish embryo from 30 to 43 hpf. (**A-A″**) Global views of the trunk region at 30 hpf. (**B-K**) Three VAE cells expressing *scl-β:d2eGFP* are seen to undergo EHT and subsequently enter circulation through the axial vein. Also see supplementary material Movie 2. Dashed circles and arrows (F,J,K) indicate HSCs that disappear from the AGM and enter into circulation. White arrows (A″,K) indicate the direction of the blood stream in the dorsal aorta. Scale bars: 30 μm in A-A″; 20 μm in B-K.

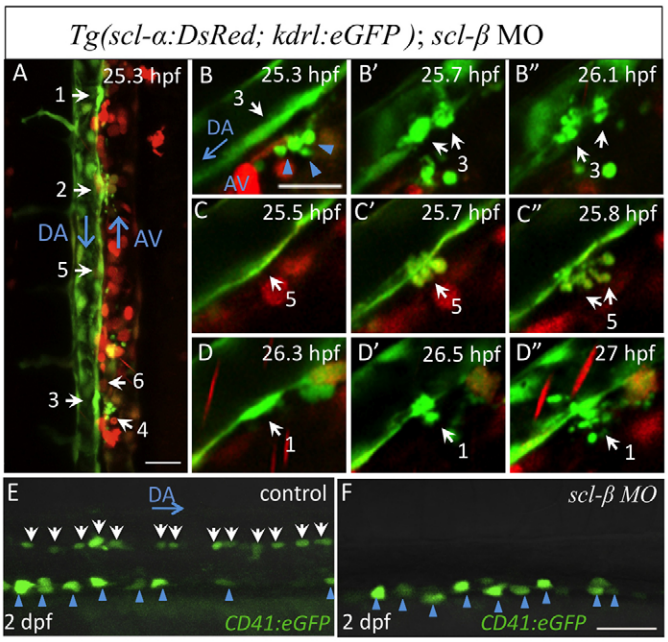

Fig. 4. *scl-β* is crucial for hemogenic endothelium specification. (**A-D″**) Time-lapse confocal imaging of a live *Tg(scl-α:DsRed; kdrl:eGFP) scl-β* zebrafish morphant from 25 to 36 hpf. White arrows and numbers indicate the endothelial cells that will undergo fragmentation during the following 6 hours. In B-D″, three *kdrl:eGFP*$^+$ elongated endothelial cells burst into fragments without initiation of budding. Also see supplementary material Movie 3. Blue arrowheads in B indicate some cell debris that already existed before recording. Similar results were obtained in all three *scl-β* morphants observed (*n*=3/3). (**E**,**F**) *CD41:eGFP*$^+$ HSCs in the AGM region of 2 dpf live control embryos and *scl-β* morphants. On average, fewer than one *CD41:eGFP*$^+$ HSC could be detected in the AGM of *scl-β* morphants (*n*=17/19), compared with an average of 13 *CD41:eGFP*$^+$ HSCs (white arrows) in the same region of control embryos. Blue arrowheads identify pronephric duct cells. Scale bars: 30 μm in A; 20 μm in B-F.

TUNEL staining indicated that the fragmented *kdrl:eGFP*$^+$ VAE cells were undergoing apoptosis (supplementary material Fig. S4I-N). These events occurred in single endothelial cells throughout the entire dorsal aorta, and were detected as early as 25 hpf (data not shown) and continued until 31 hpf (supplementary material Movie 3). Consistent with the fragmentation occurring before EHT, these apoptotic *kdrl:eGFP*$^+$ cells were of the elongated endothelial cell shape, and none showed any morphological sign of EHT (Fig. 4B-D″; supplementary material Movie 3). As a result, the *CD41:eGFP*$^+$ HSCs were almost undetectable in *scl-β* morphants (Fig. 4E,F). The loss of the HSC phenotype could be partially rescued by introducing a PAC expressing *scl-β*, demonstrating the specificity of *scl-β* MO targeting (supplementary material Fig. S4E-H). This endothelial cell apoptosis phenotype was not associated with any gross impairment in vascular differentiation, as shown by the normal expression of *kdrl:eGFP* (Fig. 4A), the vessel-specific marker *fli1* (Brown et al., 2000), and the artery-specific marker *dll4* (Leslie et al., 2007), as well as the normal growth of intersegmental vessels in *scl-β*-deficient embryos (supplementary material Fig. S4A-D; data not shown). Rather, it reflected the selective loss of hemogenic endothelial cells in *scl-β*-deficient embryos (Fig. 4E,F; supplementary material Movie 3). Altogether, our data suggest that *scl-β* deficiency inhibits HSC formation in the AGM by depleting the hemogenic endothelium.

scl-α is required for the maintenance of HSCs in the AGM

Given that the expression of *scl-α:DsRed* colocalized with the HSC-associated markers *cmyb:eGFP* and *CD41:eGFP* in the AGM (Fig. 2J-O), we further correlated the *scl-α:DsRed* expression with EHT progression by time-lapse imaging of *Tg(scl-α:DsRed; kdrl:eGFP)* embryos. As EHT proceeded, *scl-α:DsRed* expression increased and became abundant in the mature HSCs in the AGM. Such correlated expression of *scl-α:DsRed* with EHT was observed in all 34 EHT events scored in four embryos (Fig. 5A-D″; supplementary material Table S2). Thus, these results suggest that the expression of *scl-α* in the AGM is intimately associated with the emergence of HSCs from VAE.

We next examined the role of *scl-α* in HSC development. As previously reported (Qian et al., 2007), the expression of *cmyb* in the AGM of *scl-α* morphants was indistinguishable from that of controls at 26 hpf (Fig. 6A,D). However, whereas *cmyb* expression persisted until 2 dpf in control embryos, it decreased rapidly in *scl-α* morphants, being approximately half of that in control embryos at 40 hpf (Fig. 6B,E). Similar results were obtained through scoring *CD41:eGFP*$^+$ cells in the AGM of *Tg(CD41:eGFP) scl-α* morphants (Fig. 6G,H). Consistent with the reduction of HSCs in the AGM, the expression of *cmyb* in the CHT was greatly reduced by 3 dpf in *scl-α* morphants (Fig. 6C,F). This phenotype could be

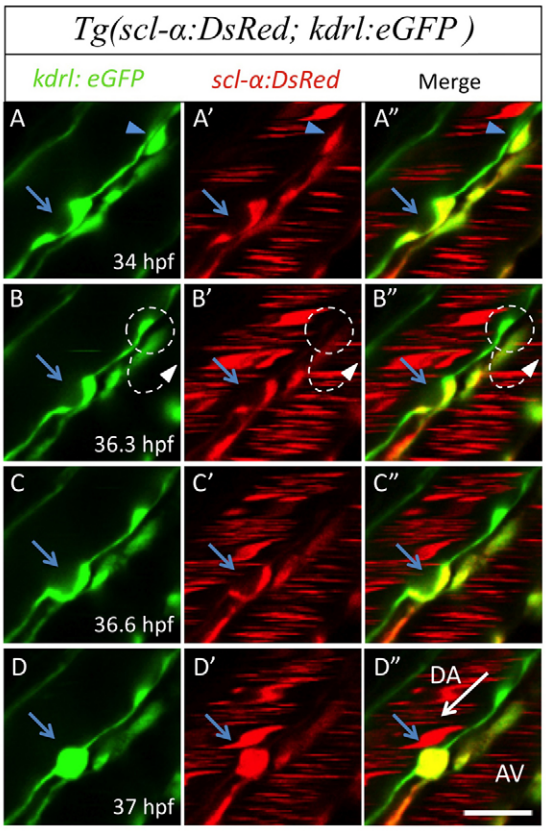

Fig. 5. Expression of *scl-α:DsRed* correlates with EHT. (**A-D″**) Time-lapse confocal imaging of a live *Tg*(*scl-α:DsRed; kdrl:eGFP*) zebrafish embryo from 34 to 37 hpf. Selected planes are presented to show EHT of an *scl-α:DsRed*$^{+}$*/kdrl:eGFP*$^{+}$ cell (blue arrows). An *scl-α:DsRed*$^{+}$*/kdrl:eGFP*$^{+}$ cell in the AGM before recording (A-A″, blue arrowheads) enters circulation shortly after (B-B″, dashed circles and arrows). White arrow (D″) indicates the direction of blood flow in the dorsal aorta. Scale bar: 20 μm.

partially rescued by the introduction of a PAC expressing *scl-α*, demonstrating the specificity of *scl-α* MO targeting (supplementary material Fig. S5A-C). To explore the underlying cellular basis for this reduction in AGM HSCs, we monitored HSC development in the AGM of live *Tg*(*scl-α:DsRed; kdrl:eGFP*) *scl-α* morphants (Fig. 6I-L″; supplementary material Movie 4). In *scl-α* morphants, *scl-α:DsRed*$^{+}$*/kdrl:eGFP*$^{+}$ HSCs formed normally from endothelial cells. However, after a relatively long stay of 6-8 hours in the subaortic space, the *scl-α:DsRed*$^{+}$*/kdrl:eGFP*$^{+}$ HSCs died through apoptosis at ~41-50 hpf (Fig. 6I-L″; supplementary material Fig. S5D-I, Movie 4). Therefore, largely consistent with its expression by emerging and nascent HSCs, our data indicate that *scl-α* is required for the maintenance of HSCs in the AGM.

Scl-β, Runx1 and Scl-α constitute a molecular hierarchy regulating sequential steps of AGM HSC development

Previous studies have shown that EHT events are impaired in *runx1*-deficient embryos (Kissa and Herbomel, 2010), suggesting that *runx1* is essential for EHT. However, whether Runx1 has a contributing pre-EHT role in AGM HSC development is not known. To address this, we examined the impact of *runx1* deficiency on HSC development in detail. By time-lapse imaging *Tg*(*scl-α:DsRed; kdrl:eGFP*) embryos injected with *runx1* MO, we found that prior to EHT (24-30 hpf), the endothelial cell apoptosis seen in *scl-β* morphants (Fig. 4A-D″; supplementary material Movie 3) was not observed in *runx1* morphants. Consistently, the hemogenic endothelial cell population marked by *scl-β* was not affected in *runx*^{w84x} mutants (Fig. 7A,B). At the time of active ongoing EHT in controls (30-40 hpf), in *runx1* morphants some of the *kdrl:eGFP*$^{+}$ endothelial cells did initiate EHT by bending ventrally but then burst into fragments as they rounded up. In accordance with some initiation of EHT in *runx1* morphants, *scl-α:DsRed* expression was observed in the apoptotic *kdrl:eGFP*$^{+}$ endothelial cells (Fig. 7C-E″; supplementary material Movie 5).

Overall, these results suggest that *runx1* specifically regulates EHT without influencing the formation of hemogenic endothelium. Based on the timing at which the apoptosis phenotype occurred in the three morphants, and the cellular phenotypes elicited by knocking down *scl-β*, *scl-α* and *runx1*, we concluded that *scl-β*, *runx1* and *scl-α* act at distinct, but sequential, steps during AGM HSC development: *scl-β* first confers hemogenic potential to a selective subset of VAE cells, *runx1* then transforms hemogenic endothelial cells into HSCs, and *scl-α* finally maintains newly born AGM HSCs (Fig. 7F).

DISCUSSION

The promise of HSC-based therapy has brought about a long-standing interest in how HSCs normally arise during embryogenesis. Over recent years, joint experimental efforts in multiple species have provided compelling evidence for the emergence of HSCs from the AGM region. A recent breakthrough came with studies showing that HSCs directly transit from a subset of aortic endothelial cells, namely the hemogenic endothelium (Bertrand et al., 2010; Boisset et al., 2010; Kissa and Herbomel, 2010; Lam et al., 2010). Although a number of transcription factors have been implicated in the development of AGM HSCs, primarily by mouse gene-targeting studies, few have been characterized in terms of mapping their function to defined stages of HSC development. In the current study, using high-resolution *in vivo* time-lapse imaging to make observations that might otherwise not be possible by conventional methods, we documented distinct cellular and developmental defects leading to the same loss of AGM HSCs in *scl-β*-, *scl-α*- or *runx1*-deficient embryos. Inferred from these phenotypes and their consistent occurrence, we defined three distinct but sequential steps in the development of AGM HSCs, each of which is uniquely regulated by one of these three factors: hemogenic endothelium is first specified by *scl-β*, the emergence of HSCs from hemogenic endothelium is then controlled by *runx1*, and finally nascent HSCs are sustained by *scl-α*. Thus, for the first time, the exact developmental stage at which *scl* or *scl* isoforms act to regulate AGM HSCs is defined. Along with previous results showing that cMyb is indispensable for the egression of HSCs from the AGM (Zhang et al., 2011), we propose a transcription factor relay that coordinates the orderly progression of AGM HSC development from hemogenic endothelium to regulated HSC exit (Fig. 7F). In mammalian systems, the N-terminal-truncated SCL isoform corresponding to zebrafish Scl-β was reported to be expressed in certain human T-cell leukemia cell lines (Bernard et al., 1992; Pulford et al., 1995). However, the expression and specific function of full-length and truncated mammalian SCL isoforms in the context of hemogenic endothelium formation and HSC development have not been explored. Considering the high similarity between zebrafish and mammalian hematopoiesis in terms of molecular regulation, our research provides a framework to untangle isoform-specific roles of mammalian SCL isoforms in HSC formation.

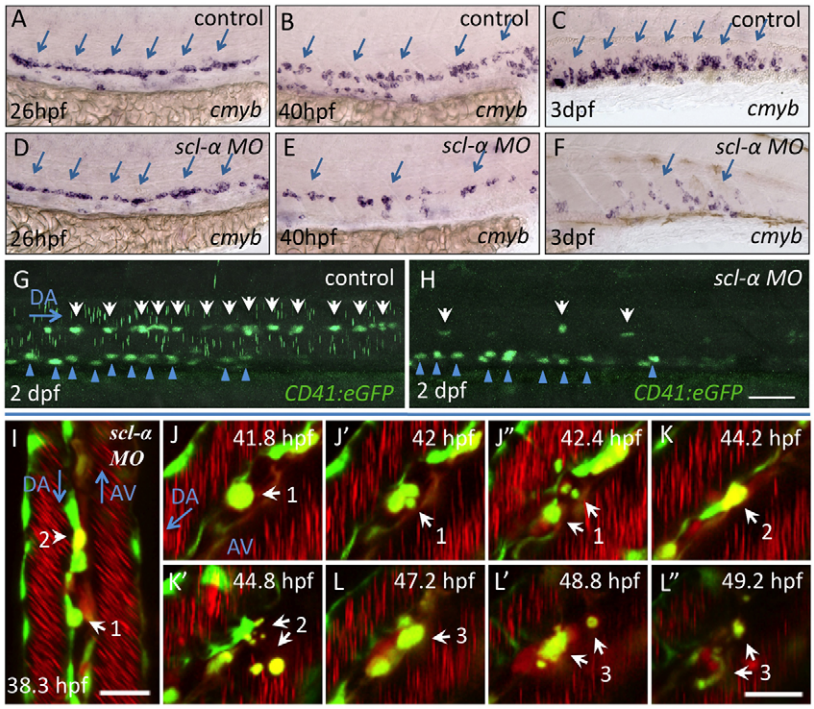

Fig. 6. *scl-α* is required for the maintenance of HSCs in the AGM. (**A-F**) *cmyb* expression in control zebrafish embryos and *scl-α* morphants. Arrows indicate *cmyb* expression in AGM (A,B,D,E) or CHT (C,F) region. D, *n*=43/48; E, *n*=37/45; F, *n*=34/40. (**G**,**H**) *CD41:eGFP*$^{+}$ HSCs in the AGM of 2 dpf control embryos and *scl-α* morphants (*n*=25/28). White arrows identify the *CD41:eGFP*$^{+}$ HSCs and blue arrowheads indicate unaffected *CD41:eGFP*$^{+}$ cells in the pronephric duct. (**I-L″**) Time-lapse confocal imaging of a live *Tg*(*scl-α:DsRed; kdrl:eGFP*) embryo injected with *scl-α* MO from ~38 to 50 hpf. In J-L″, selected planes show three apoptotic HSCs in the *scl-α* morphants. Also see supplementary material Movie 4. Similar results were obtained in all four *scl-α* morphants observed (*n*=4/4). Scale bars: 50 μm in G,H; 20 μm in I-L″.

Our data show that prior to the onset of EHT and blood flow, *scl-β* is expressed in a selective subset of VAE cells destined to become HSCs and is functionally required for the formation of these cells. Remarkably, only the *scl-β*$^{+}$ VAE subset, and not the remaining *scl-β*$^{-}$ cells, gives rise to HSCs via EHT. This suggests that hemogenic potential is not widely distributed across the entire VAE but is restricted to a defined subpopulation, and is thus in support of the emergence of HSCs from VAE as a deterministic rather than stochastic event. To our knowledge, *scl-β* is the first molecular determinant for hemogenic endothelial cells, a crucial intermediate

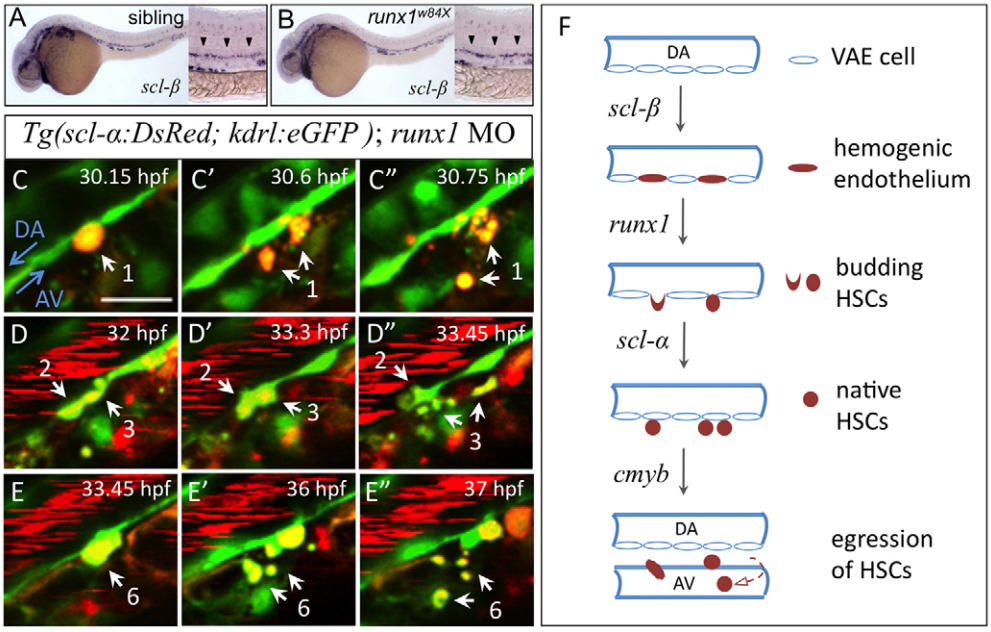

Fig. 7. Scl-β, Runx1 and Scl-α regulate sequential steps of AGM HSC development. (**A**,**B**) Hemogenic endothelium marked by *scl-β* expression in 28 hpf siblings (heterozygotes and wild type) and *runx1*^{w84x} mutant zebrafish embryos. Arrowheads indicate expression of *scl-β* in the AGM region. (**C-E″**) Time-lapse confocal imaging of a live *Tg*(*scl-α:DsRed; kdrl:eGFP*) embryo injected with *runx1* MO from 32 to 39 hpf. White arrows indicate four *scl-α:DsRed*$^{+}$ VAE cells that initiate budding but then fragment. Also see supplementary material Movie 5. Similar results were obtained in all three of the *runx1* morphants examined and a total of 13 such events were observed (*n*=3/3). Scale bars: 20 μm. (**F**) A model of the molecular regulation at consecutive steps during the development of HSCs in the AGM. The establishment of hemogenic endothelium relies on *scl-β*. *runx1* is crucial for their subsequent transformation into HSCs via EHT. The maintenance of nascent HSCs in the AGM requires *scl-α*, and *cmyb* is essential to regulate the egression of these HSCs from the AGM.

in the development of AGM HSCs, providing a genetic handle for further study of this important, yet less well understood, cell population. An intriguing observation is that, although the vast majority (80%) of the *scl-β:eGFP*$^{+}$ VAE cells give rise to HSCs via EHT, ~20% of them gradually lose *scl-β* expression (data not shown), at least during the imaging period (from 28 to 54 hpf), and presumably remain as aortic endothelial cells thereafter. This implies that a larger endothelial cell population (*scl-β*$^{+}$) might initially acquire hemogenic potential to support HSC generation and that they might also lose their hemogenic potential when not needed. In light of the rapid development of early zebrafish embryos, this redundancy and plasticity of endothelial to hematopoietic conversion might ensure that a sufficient number of HSCs is produced within a short permissive time window without compromising vascular integrity.

We show that *runx1* is dispensable for hemogenic endothelium formation but becomes essential upon the transformation of endothelial cells into HSCs. Together with a previous study reporting that deletion of *runx1* immediately after the completion of EHT has no effect on HSCs (Chen et al., 2009), we suggest that, during the emergence of HSCs, *runx1* is only required at the stage of EHT, and not before or thereafter. It is currently unknown whether *scl-β* is also required for the activation of the EHT program besides acting in the formation of hemogenic endothelium. It is plausible that *scl-β* might prime hemogenic endothelium for EHT by activating the expression of *runx1*. Prior work in mouse has suggested that SCL directly regulates *Runx1* promoter activity during yolk sac and fetal liver hematopoiesis, unconventionally through GATA2 binding sites rather than SCL binding sites (Porcher et al., 1999; Landry et al., 2008). Further studies have shown that GATA/ETS/SCL motifs in a +23 enhancer element control RUNX1-mediated HSC emergence (Nottingham et al., 2007; Ng et al., 2010). In zebrafish, however, cis-regulatory elements that govern *runx1* expression in HSCs remain poorly defined, although two large genomic fragments encompassing *runx1* distal and proximal promoters have been shown to label distinct definitive hematopoietic progenitors (Lam et al., 2009). The mouse *Runx1* +23 enhancer can direct reporter expression in HSCs in zebrafish embryos (our unpublished data), making it likely that an analogous *scl-runx1* regulatory mechanism might operate in zebrafish.

Finally, our study has uncovered a previously unidentified role of *scl-α* in maintaining HSCs in the AGM. This role of *scl-α* is supported by the findings that the depletion of HSC-associated markers in AGM, CHT and pronephros follows a normal EHT, and the normal initial expression of these markers in the AGM in *scl-α* morphants. However, in contrast to the severe loss of HSCs in CHT and pronephros, T-cell development is marginally affected, as *rag1* expression in the thymus is either unaffected or only slightly reduced in *scl-α* morphants as compared with controls (Qian et al., 2007) (supplementary material Fig. S6). Accordingly, we observed that a few *scl-α:DsRed*$^{+}$*/kdrl:eGFP*$^{+}$ HSCs were released into the circulation after 60 hpf in *scl-α* morphants (data not shown). Unlike gene knockout, MO-mediated knockdown tends to be incomplete. As such, a possible explanation for the spared T-cell development could be the insensitivity of this lineage to the incomplete suppression of *scl-α*, for example through the compensatory proliferation or differentiation of residual hematopoietic progenitors in the thymus of *scl-α* morphants. Alternatively, this might be attributed to the *scl-α*-independent emergence of the first T-cells in developing embryos. It is plausible that the first T-cells are produced from 32 to 40 hpf, when HSC markers are normally expressed in the AGM of *scl-α* morphants. Clarification of this issue would benefit from the creation of a zebrafish line stably deleted for the *scl-α* isoform.

Collectively, our findings demonstrate the importance of the orderly action of the transcription factors *scl-β*, *runx1* and *scl-α* in the progressive development of HSCs from the AGM in vertebrates. These results have direct implications for the quest to derive blood cells from endothelial cells or induced pluripotent stem cells (Szabo et al., 2010).

Acknowledgements
We thank Hao Jin for scientific discussion and critical comments on the manuscript; and R. Handin and L. Zon for providing *Tg(cd41:eGFP)* and *Tg(cmyb:eGFP)* transgenic lines.

Funding
This work was supported by the National Basic Research Program of China [grant 2012CB945102], by the National Natural Science Foundation of China [grants 31171403 and 30828020], and by General Research Fund (GRF) grants from the Research Grants Council of the Hong Kong Special Administrative Region [grants HKUST6/CRF/09, 663111 and 663212].

Competing interests statement
The authors declare no competing financial interests.

Author contributions
F.Z., Y.L. and B.Y. designed the research, performed experiments and analyzed data. W.Z. and Z.W. designed the research and analyzed data.

Supplementary material
Supplementary material available online at
http://dev.biologists.org/lookup/suppl/doi:10.1242/dev.097071/-/DC1

References

Bernard, O., Azogui, O., Lecointe, N., Mugneret, F., Berger, R., Larsen, C. J. and Mathieu-Mahul, D. (1992). A third tal-1 promoter is specifically used in human T cell leukemias. *J. Exp. Med.* **176**, 919-925.
Bertrand, J. Y., Chi, N. C., Santoso, B., Teng, S., Stainier, D. Y. and Traver, D. (2010). Haematopoietic stem cells derive directly from aortic endothelium during development. *Nature* **464**, 108-111.
Bevis, B. J. and Glick, B. S. (2002). Rapidly maturing variants of the Discosoma red fluorescent protein (DsRed). *Nat. Biotechnol.* **20**, 83-87.
Boisset, J. C., van Cappellen, W., Andrieu-Soler, C., Galjart, N., Dzierzak, E. and Robin, C. (2010). In vivo imaging of haematopoietic cells emerging from the mouse aortic endothelium. *Nature* **464**, 116-120.
Brown, L. A., Rodaway, A. R., Schilling, T. F., Jowett, T., Ingham, P. W., Patient, R. K. and Sharrocks, A. D. (2000). Insights into early vasculogenesis revealed by expression of the ETS-domain transcription factor Fli-1 in wild-type and mutant zebrafish embryos. *Mech. Dev.* **90**, 237-252.
Burns, C. E., Traver, D., Mayhall, E., Shepard, J. L. and Zon, L. I. (2005). Hematopoietic stem cell fate is established by the Notch-Runx pathway. *Genes Dev.* **19**, 2331-2342.
Chen, M. J., Yokomizo, T., Zeigler, B. M., Dzierzak, E. and Speck, N. A. (2009). Runx1 is required for the endothelial to haematopoietic cell transition but not thereafter. *Nature* **457**, 887-891.
Dooley, K. A., Davidson, A. J. and Zon, L. I. (2005). Zebrafish scl functions independently in hematopoietic and endothelial development. *Dev. Biol.* **277**, 522-536.
Eilken, H. M., Nishikawa, S. and Schroeder, T. (2009). Continuous single-cell imaging of blood generation from haemogenic endothelium. *Nature* **457**, 896-900.
Gering, M. and Patient, R. (2005). Hedgehog signaling is required for adult blood stem cell formation in zebrafish embryos. *Dev. Cell* **8**, 389-400.
Gering, M., Rodaway, A. R. F., Göttgens, B., Patient, R. K. and Green, A. R. (1998). The SCL gene specifies haemangioblast development from early mesoderm. *EMBO J.* **17**, 4029-4045.
Green, A. R., Salvaris, E. and Begley, C. G. (1991). Erythroid expression of the 'helix-loop-helix' gene, SCL. *Oncogene* **6**, 475-479.
Green, A. R., Lints, T., Visvader, J., Harvey, R. and Begley, C. G. (1992). SCL is coexpressed with GATA-1 in hemopoietic cells but is also expressed in developing brain. *Oncogene* **7**, 653-660.
Hwang, L. Y., Siegelman, M., Davis, L., Oppenheimer-Marks, N. and Baer, R. (1993). Expression of the TAL1 proto-oncogene in cultured endothelial cells and blood vessels of the spleen. *Oncogene* **8**, 3043-3046.
Jin, S. W., Beis, D., Mitchell, T., Chen, J. N. and Stainier, D. Y. (2005). Cellular and molecular analyses of vascular tube and lumen formation in zebrafish. *Development* **132**, 5199-5209.

Jin, H., Xu, J. and Wen, Z. (2007). Migratory path of definitive hematopoietic stem/progenitor cells during zebrafish development. *Blood* **109**, 5208-5214.
Jin, H., Sood, R., Xu, J., Zhen, F., English, M. A., Liu, P. P. and Wen, Z. (2009). Definitive hematopoietic stem/progenitor cells manifest distinct differentiation output in the zebrafish VDA and PBI. *Development* **136**, 647-654.
Kallianpur, A. R., Jordan, J. E. and Brandt, S. J. (1994). The SCL/TAL-1 gene is expressed in progenitors of both the hematopoietic and vascular systems during embryogenesis. *Blood* **83**, 1200-1208.
Kimmel, C. B., Ballard, W. W., Kimmel, S. R., Ullmann, B. and Schilling, T. F. (1995). Stages of embryonic development of the zebrafish. *Dev. Dyn.* **203**, 253-310.
Kissa, K. and Herbomel, P. (2010). Blood stem cells emerge from aortic endothelium by a novel type of cell transition. *Nature* **464**, 112-115.
Kissa, K., Murayama, E., Zapata, A., Cortés, A., Perret, E., Machu, C. and Herbomel, P. (2008). Live imaging of emerging hematopoietic stem cells and early thymus colonization. *Blood* **111**, 1147-1156.
Lam, E. Y. N., Chau, J. Y. M., Kalev-Zylinska, M. L., Fountaine, T. M., Mead, R. S., Hall, C. J., Crosier, P. S., Crosier, K. E. and Flores, M. V. (2009). Zebrafish runx1 promoter-EGFP transgenics mark discrete sites of definitive blood progenitors. *Blood* **113**, 1241-1249.
Lam, E. Y., Hall, C. J., Crosier, P. S., Crosier, K. E. and Flores, M. V. (2010). Live imaging of Runx1 expression in the dorsal aorta tracks the emergence of blood progenitors from endothelial cells. *Blood* **116**, 909-914.
Lancrin, C., Sroczynska, P., Stephenson, C., Allen, T., Kouskoff, V. and Lacaud, G. (2009). The haemangioblast generates haematopoietic cells through a haemogenic endothelium stage. *Nature* **457**, 892-895.
Landry, J. R., Kinston, S., Knezevic, K., de Bruijn, M. F. T. R., Wilson, N., Nottingham, W. T., Peitz, M., Edenhofer, F., Pimanda, J. E., Ottersbach, K. et al. (2008). Runx genes are direct targets of Scl/Tal1 in the yolk sac and fetal liver. *Blood* **111**, 3005-3014.
Lee, C. Y., Vogeli, K. M., Kim, S. H., Chong, S. W., Jiang, Y. J., Stainier, D. Y. and Jin, S. W. (2009). Notch signaling functions as a cell-fate switch between the endothelial and hematopoietic lineages. *Curr. Biol.* **19**, 1616-1622.
Leslie, J. D., Ariza-McNaughton, L., Bermange, A. L., McAdow, R., Johnson, S. L. and Lewis, J. (2007). Endothelial signalling by the Notch ligand Delta-like 4 restricts angiogenesis. *Development* **134**, 839-844.
Lin, H. F., Traver, D., Zhu, H., Dooley, K., Paw, B. H., Zon, L. I. and Handin, R. I. (2005). Analysis of thrombocyte development in CD41-GFP transgenic zebrafish. *Blood* **106**, 3803-3810.
Murayama, E., Kissa, K., Zapata, A., Mordelet, E., Briolat, V., Lin, H. F., Handin, R. I. and Herbomel, P. (2006). Tracing hematopoietic precursor migration to successive hematopoietic organs during zebrafish development. *Immunity* **25**, 963-975.
Ng, C. E. L., Yokomizo, T., Yamashita, N., Cirovic, B., Jin, H., Wen, Z., Ito, Y. and Osato, M. (2010). A Runx1 intronic enhancer marks hemogenic endothelial cells and hematopoietic stem cells. *Stem Cells* **28**, 1869-1881.
North, T. E., Goessling, W., Walkley, C. R., Lengerke, C., Kopani, K. R., Lord, A. M., Weber, G. J., Bowman, T. V., Jang, I. H., Grosser, T. et al. (2007). Prostaglandin E2 regulates vertebrate haematopoietic stem cell homeostasis. *Nature* **447**, 1007-1011.
Nottingham, W. T., Jarratt, A., Burgess, M., Speck, C. L., Cheng, J. F., Prabhakar, S., Rubin, E. M., Li, P. S., Sloane-Stanley, J., Kong-A-San, J. et al. (2007). Runx1-mediated hematopoietic stem-cell emergence is controlled by a Gata/Ets/SCL-regulated enhancer. *Blood* **110**, 4188-4197.
Orkin, S. H. and Zon, L. I. (2008). Hematopoiesis: an evolving paradigm for stem cell biology. *Cell* **132**, 631-644.
Patterson, L. J., Gering, M. and Patient, R. (2005). Scl is required for dorsal aorta as well as blood formation in zebrafish embryos. *Blood* **105**, 3502-3511.
Porcher, C., Swat, W., Rockwell, K., Fujiwara, Y., Alt, F. W. and Orkin, S. H. (1996). The T cell leukemia oncoprotein SCL/tal-1 is essential for development of all hematopoietic lineages. *Cell* **86**, 47-57.
Porcher, C., Liao, E. C., Fujiwara, Y., Zon, L. I. and Orkin, S. H. (1999). Specification of hematopoietic and vascular development by the bHLH transcription factor SCL without direct DNA binding. *Development* **126**, 4603-4615.
Pulford, K., Lecointe, N., Leroy-Viard, K., Jones, M., Mathieu-Mahul, D. and Mason, D. Y. (1995). Expression of TAL-1 proteins in human tissues. *Blood* **85**, 675-684.
Qian, F., Zhen, F., Xu, J., Huang, M., Li, W. and Wen, Z. (2007). Distinct functions for different scl isoforms in zebrafish primitive and definitive hematopoiesis. *PLoS Biol.* **5**, e132.
Rembold, M., Lahiri, K., Foulkes, N. S. and Wittbrodt, J. (2006). Transgenesis in fish: efficient selection of transgenic fish by co-injection with a fluorescent reporter construct. *Nat. Protoc.* **1**, 1133-1139.
Ren, X., Gomez, G. A., Zhang, B. and Lin, S. (2010). Scl isoforms act downstream of etsrp to specify angioblasts and definitive hematopoietic stem cells. *Blood* **115**, 5338-5346.
Robb, L., Lyons, I., Li, R., Hartley, L., Köntgen, F., Harvey, R. P., Metcalf, D. and Begley, C. G. (1995). Absence of yolk sac hematopoiesis from mice with a targeted disruption of the scl gene. *Proc. Natl. Acad. Sci. USA* **92**, 7075-7079.
Robb, L., Elwood, N. J., Elefanty, A. G., Köntgen, F., Li, R., Barnett, L. D. and Begley, C. G. (1996). The scl gene product is required for the generation of all hematopoietic lineages in the adult mouse. *EMBO J.* **15**, 4123-4129.
Robin, C., Ottersbach, K., Durand, C., Peeters, M., Vanes, L., Tybulewicz, V. and Dzierzak, E. (2006). An unexpected role for IL-3 in the embryonic development of hematopoietic stem cells. *Dev. Cell* **11**, 171-180.
Shivdasani, R. A., Mayer, E. L. and Orkin, S. H. (1995). Absence of blood formation in mice lacking the T-cell leukaemia oncoprotein tal-1/SCL. *Nature* **373**, 432-434.
Sood, R., English, M. A., Belele, C. L., Jin, H., Bishop, K., Haskins, R., McKinney, M. C., Chahal, J., Weinstein, B. M., Wen, Z. et al. (2010). Development of multilineage adult hematopoiesis in the zebrafish with a runx1 truncation mutation. *Blood* **115**, 2806-2809.
Szabo, E., Rampalli, S., Risueño, R. M., Schnerch, A., Mitchell, R., Fiebig-Comyn, A., Levadoux-Martin, M. and Bhatia, M. (2010). Direct conversion of human fibroblasts to multilineage blood progenitors. *Nature* **468**, 521-526.
Visvader, J. E., Fujiwara, Y. and Orkin, S. H. (1998). Unsuspected role for the T-cell leukemia protein SCL/tal-1 in vascular development. *Genes Dev.* **12**, 473-479.
Yang, Z., Jiang, H., Chaichanasakul, T., Gong, S., Yang, X. W., Heintz, N. and Lin, S. (2006). Modified bacterial artificial chromosomes for zebrafish transgenesis. *Methods* **39**, 183-188.
Zhang, X. Y. and Rodaway, A. R. F. (2007). SCL-GFP transgenic zebrafish: in vivo imaging of blood and endothelial development and identification of the initial site of definitive hematopoiesis. *Dev. Biol.* **307**, 179-194.
Zhang, Y., Jin, H., Li, L., Qin, F. X. and Wen, Z. (2011). cMyb regulates hematopoietic stem/progenitor cell mobilization during zebrafish hematopoiesis. *Blood* **118**, 4093-4101.